JOURNAL OF MATERIALS SCIENCE 28 (1993) 742–752

Evaluation of R-curve effects in ceramics

T. FETT, D. MUNZ
Kernforschungszentrum Karlsruhe, Institut für Materialforschung II, and Institut für Zuverlässigkeit und Schadenskunde im Maschinenbau, Universität Karlsruhe, Postfach 3640, W 7500 Karlsruhe, Germany

In coarse-grained alumina the crack growth resistance increases with increasing crack extension due to crack–border interactions. The crack shielding stress intensity factor can be calculated from the relation between the bridging stresses and the crack opening displacement. The parameters of this relation can be obtained from experimental results on stable or subcritical crack extension. Finally the effect of the R-curve on the behaviour of components with small cracks is discussed.

1. Introduction

Coarse-grained Al_2O_3 shows an R-curve behaviour which is characterized by an increase in crack growth resistance with increasing crack extension [1–10]. It was demonstrated experimentally [2, 3] that this effect is caused by crack–border interactions in the wake of the advancing crack. Recently, the crack–surface interactions have been detected *in situ* under the electron microscope [11, 12]. The bridging interactions were observed mainly on large grains.

Crack shielding by crack–border interaction is not only effective in a test involving increasing load. Also under constant load with subcritical crack growth the crack–border interaction affects the observed crack growth rate. The stress intensity factor acting at the crack tip, K_{Itip}, can be written as

$$K_{\mathrm{Itip}} = K_{\mathrm{Iappl}} - K_{\mathrm{Ibr}} \tag{1}$$

where K_{Iappl} is calculated from the external load, neglecting crack–border interaction, and K_{Ibr} is caused by the compressive bridging stresses.

In the first part of the paper an appropriate bridging stress relation is established. Then the general influence of the bridging stresses on the R-curve behaviour of macro-cracks is studied for stable and subcritical crack growth. In three examples the parameters of the bridging law are determined from experimental literature results. After describing the general R-curve behaviour of small cracks, a procedure is presented that allows one to determine the bridging parameters of natural cracks.

2. The bridging stress relation

The bridging stresses are dependent on the crack opening displacement δ. Mai and Lawn [13] proposed a relation

$$\sigma_{\mathrm{br,grain}} = \begin{cases} \sigma_0[1-(\delta/\delta_0)]^m & \text{for } \delta/\delta_0 < 1 \\ 0 & \text{for } \delta/\delta_0 > 1 \end{cases} \qquad m = 0, 1, 2, \ldots \tag{2}$$

that is shown in Fig. 1. It is assumed that the characteristic displacement for which the bridging stresses vanish is proportional to the grain size. On account of grain size distribution, the characteristic displacement is also distributed.

It is assumed that the distribution density of δ_0 is a Γ-distribution, as represented in Fig. 2.

$$f(\delta_0) = \frac{1}{\delta_{00}}\left(\frac{\delta_0}{\delta_{00}}\right)\exp\left(-\frac{\delta_0}{\delta_{00}}\right) \tag{3}$$

Other Γ-distributions are considered elsewhere [14]. The macroscopically averaged bridging stresses result from

$$\sigma_{\mathrm{br,aver}} = \int_0^\infty \sigma_{\mathrm{br,grain}} f(\delta_0)\,\mathrm{d}\delta_0 \tag{4}$$

For the Γ-distribution (Equation 3) the following averaged bridging stress relations result:

$$\sigma_{\mathrm{br,aver}} = \sigma_0 g(\delta/\delta_{00}) \tag{5}$$

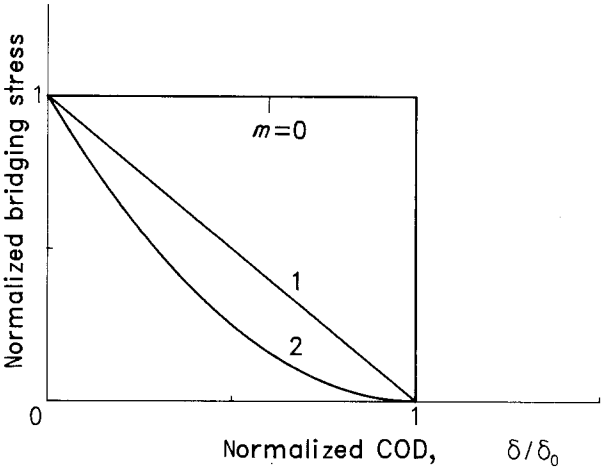

Figure 1 Stress-displacement relations for a single-grain $\sigma_{\mathrm{br}}/\sigma_0 = f(\delta/\delta_0)$.

0022–2461

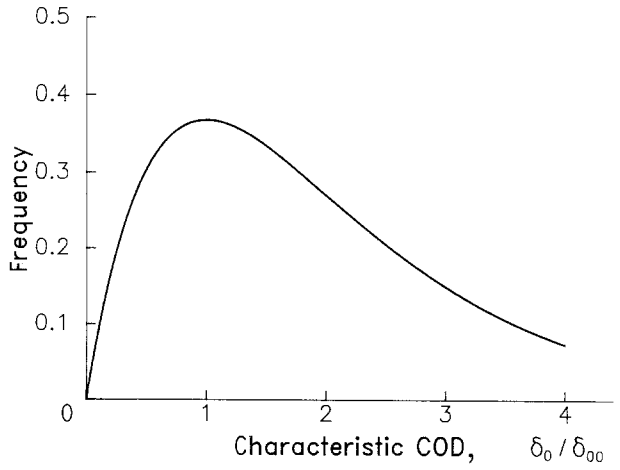

Figure 2 Distribution of the characteristic COD value δ_0 (abscissa normalized: δ_0/δ_{00}).

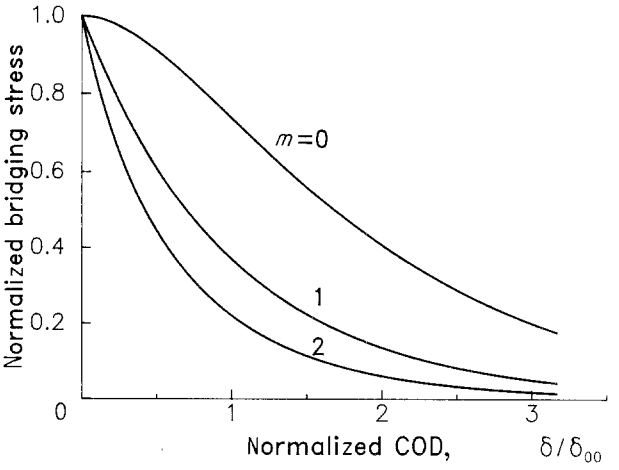

Figure 3 Influence of the parameter m in Equation 2 on the averaged bridging stress.

with

$$g(z) = (1 + z)\exp(-z) \qquad m = 0 \qquad (5.1)$$

$$g(z) = \exp(-z) \qquad m = 1 \qquad (5.2)$$

$$g(z) = (1 - z)\exp(-z) + z^2\mathbf{Ei}(z) \quad m = 2 \qquad (5.3)$$

where **Ei** is the exponential integral defined by

$$\mathbf{Ei}(x) = \int_x^\infty \frac{e^{-t}}{t}\,dt \qquad x > 0 \qquad (5.4)$$

available in most computer libraries. The bridging laws are shown in Fig. 3. These relations ensure a continuously decreasing effect of crack–border interaction with decreasing displacement. Especially the case $m = 1$ is used in the subsequent calculations.

3. Calculation of the bridging stress intensity factor

A test specimen with a crack may be loaded by an external load, which leads to a stress distribution $\sigma_{appl}(x)$ at the location of the crack in the uncracked component. The geometrical quantities of such a crack are explained in Fig. 4. In the case where the material exhibits a bridging zone with crack–surface interactions, the total stress is the sum of the applied stress and the bridging stress σ_{br}, i.e.

$$\sigma_{total}(x) = \sigma_{appl}(x) - \sigma_{br}(x) \qquad (6)$$

It is convenient to use a minus sign in Equation 6 and positive values of σ_{br}. These stresses are responsible for the stress intensity factor, which is given in the representation of the weight function [15]

$$K_I = \int_0^a h\left(\frac{x}{a}, \frac{a}{W}\right)\sigma(x)\,dx \qquad (7)$$

The total displacements of the crack surface can be easily derived by the relation existing between crack surface displacements, weight function and stress intensity factor as proposed by Rice [16]:

$$h = \frac{H}{K_I}\frac{\partial\delta}{\partial a} \qquad (8)$$

with $H = E$ for plane stress and $H = E/(1 - \nu^2)$ for plane strain. Integration of this formula yields the crack–surface displacements δ caused by the stress σ [17]

$$\delta(x) = \frac{1}{H}\int_0^a \int_{\max(x,x')}^a h(a', x)h(a', x')\sigma(x')\,da'\,dx' \qquad (9)$$

where x is the coordinate with the displacement computed and x' is the location where the stress σ acts. Equation 9 can also be derived from the procedure of Paris [18] based on Castigliano's theorem. A detailed

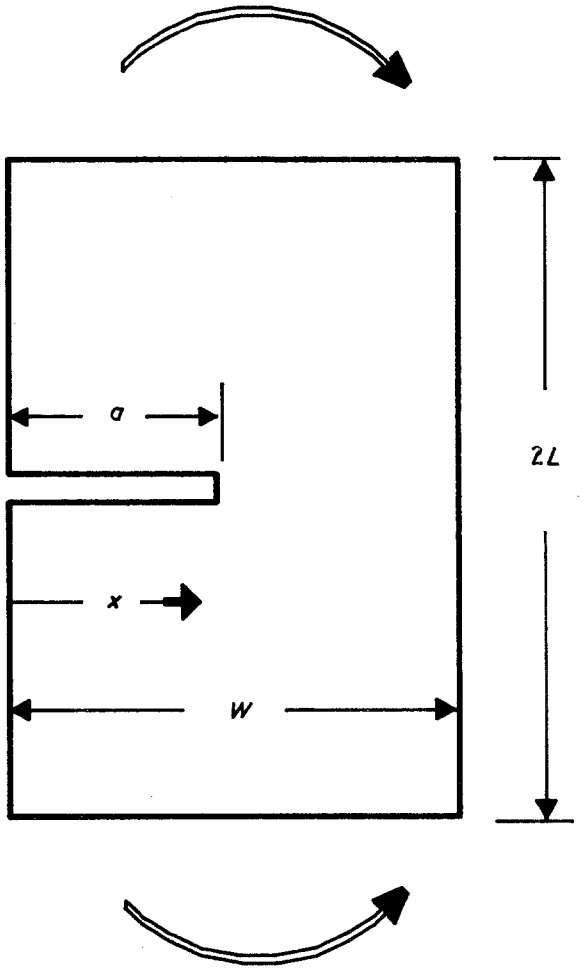

Figure 4 Specimen with a crack under bending load.

description is given in the appendix of Tada's handbook [19].

The stress intensity factors describing the R-curve behaviour can be obtained in the following way:

1. The total crack surface displacements according to the total stress (Equation 6) become

$$\delta = \frac{1}{H}\int_0^a \int_{\max(x,x')}^a h(a', x)h(a', x')(\sigma_{appl} - \sigma_{br})\,da'dx' = \delta_{00}g^{-1}(\sigma_{br}/\sigma_0) \quad (10)$$

where g^{-1} is the inverse of the function defined by Equation 5. The solution of the integral Equation 10 provides the distribution of the bridging stresses as a function of the stresses applied.

2. The related bridging stress intensity factor K_{Ibr} results from Equation 7 as

$$K_{Ibr} = \int_0^a h\left(\frac{x}{a}, \frac{a}{W}\right)\sigma_{br}(x)\,dx \quad (7.1)$$

3. The applied stress intensity factor K_{Iappl} similarly becomes

$$K_{Iappl} = \int_0^a h\left(\frac{x}{a}, \frac{a}{W}\right)\sigma_{appl}(x)\,dx \quad (7.2)$$

4. Finally, the crack tip stress intensity factor K_{Itip} is given by Equation 1.

The solution of Equation 10 can be determined by several methods. The simplest one is the iterative approximation. In the first step, the applied stress σ_{appl} is introduced in the integrand of Equation 10, yielding the crack surface displacement field δ_{appl}. A first approximation of the bridging stresses is obtained by introducing δ_{appl} in the bridging stress law. The bridging stresses obtained are then introduced once more in Equation 10 and the procedure is repeated as long as the bridging displacements are constant.

The evaluation of Equation 10 using successive approximation needs much computer time. In order to reduce the computation effort, special strategies are available [14]. The simplest one is to use tabulated solutions of the previous procedure in normalized form. These data can easily be interpolated by cubic splines.

For numerical calculations the weight function for a single-edge notched specimen [20] is recommended:

$$h_I = \left(\frac{2}{\pi a}\right)^{1/2} \frac{1}{[1-(x/a)]^{1/2}[1-(a/W)]^{3/2}} \times\left[\left(1-\frac{a}{W}\right)^{3/2} + \sum A_{\nu\mu}(1-x/a)^{\nu+1}\left(\frac{a}{W}\right)^{\mu}\right] \quad (11)$$

with the coefficients $A_{\nu\mu}$ given in Table I.

TABLE I Coefficients for Equation 11

ν \ μ	0	1	2	3	4
0	0.4980	2.4463	0.0700	1.3187	− 3.067
1	0.54165	− 5.0806	24.3447	− 32.7208	18.1214
2	− 0.19277	2.55863	− 12.6415	19.763	− 10.9860

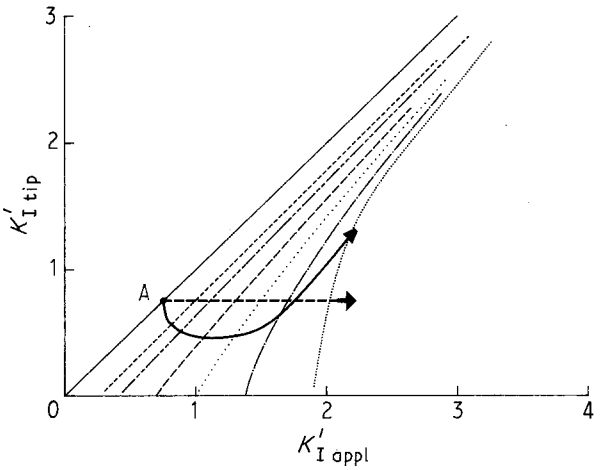

Figure 5 Stress intensity factor K'_{Itip} as a function of applied stress intensity factor K'_{Iappl} in a normalized representation (bending, $\delta'_{00} = 1$, $a_0/W = 0.5$): $a/W =$ (——) 0.50, (– – –) 0.525, (— — — —) 0.55, (— —) 0.60, (· · ·) 0.65, (— · —) 0.70, (· · · · · ·) 0.75.

4. General results

In Fig. 5 results of calculations for a crack with an initial relative crack size (e.g. a saw notch) of $a_0/W = 0.5$ under bending are represented as K_{Itip} versus. K_{Iappl} for several actual crack lengths a/W. In this figure, the stress intensity factors are normalized with respect to the maximum bridging stress σ_0 and the specimens width W as

$$K'_I = \frac{K_I}{\sigma_0 W^{1/2}} \quad (12)$$

and the parameter δ_{00} of the bridging stress relation by

$$\delta'_{00} = \frac{H}{\sigma_0 W}\delta_{00} \quad (13)$$

4.1. Constant-load tests

The representation of the stress intensity factor (Fig. 5) allows one to describe crack extension tests under different loading conditions. In Fig. 5 crack propagation in a constant-load test under subcritical crack growth conditions is illustrated by the solid line for $\sigma/\sigma_0 = 0.4$ and $\delta'_{00} = 1.0$.

The curve starts at point A corresponding to $K_{Iappl} = K_{Itip} = \sigma\ a_0^{1/2}\,Y$. With increasing crack length, first the crack-tip stress intensity factor K_{Itip} decreases and after reaching a minimum value, K_{Itip} increases monotonically. The applied stress intensity factor K_{Iappl} is plotted in Fig. 6 versus the crack extension $\Delta a/W$. The K_{Iappl}–$\Delta a/W$ curve increases monotonically. This is self-evident since for constant stress the stress intensity factor

$$K_{Iappl} = \sigma_{appl}\,a^{1/2}\,Y(a/W) \quad (14)$$

reflects only the increase in the product $a^{1/2}\,Y$ with

crack extension, and this quantity is not a material property, but depends only on the geometric data a, a/W. The bridging stress intensity factor developing with increasing crack length is traced in Fig. 7 as a solid line. A comparison between the two R-curve representations $K_{I\,br} = f(\Delta a)$ and $K_{I\,appl} = f(\Delta a)$ shows the superiority of $K_{I\,br} = f(\Delta a)$ since this representation reflects the material behaviour.

Constant-load tests for several initial stress intensity factors K_{Ii} are shown in Fig. 8. The influence of the initial stress intensity factor on the R-curve can be seen from Fig. 9. It is evident that the R-curve is more pronounced for low values of applied stress.

4.2. Crack extension with constant crack-tip stress intensity factor

In this section tests with constant stress intensity factor $K_{I\,tip}$ are considered. Such tests are difficult to perform. One possibility would be to perform tests with constant crack growth rate. Results are presented here to show the differences from the tests with constant stress. Crack extension with constant stress intensity factor $K_{I\,tip}$ (e.g. stable crack propagation with $K_{I\,tip} = K_{I0} = \text{const.}$) is described by the dashed horizontal line in Fig. 5. The related $K_{I\,appl}$–Δa curve is also shown in Fig. 6. At the beginning of crack extension, the curve is approximately square-root shaped in accordance with the literature (e.g. [21]). Also for this type of crack propagation, the R-curve representation $K_{I\,br} = f(\Delta a)$ is introduced in Fig. 7 (dashed line). For small crack extension this curve hardly deviates from the curve obtained under constant load conditions. Significant differences in the shapes of the R-curves become obvious for large crack extensions. R-curves for crack propagation at $K_{I\,tip} = \text{const.}$ are shown in Fig. 10 for different values of $K_{I\,tip}$. It becomes obvious that the R-curve depends on the level of $K_{I\,tip}$.

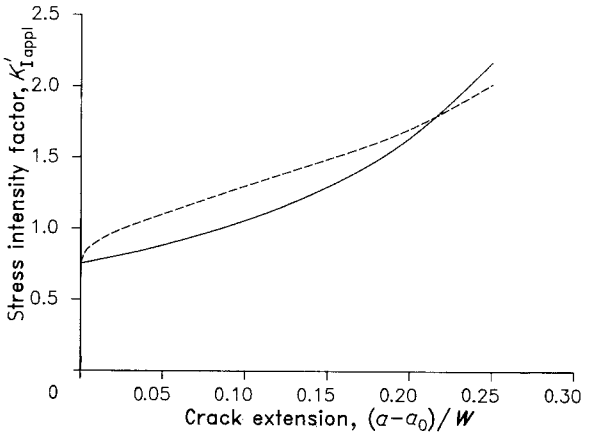

Figure 6 Applied stress intensity factor for crack extension under (——) constant load and (– – –) constant stress intensity factor $K_{I\,tip}$; $a_0/W = 0.5$.

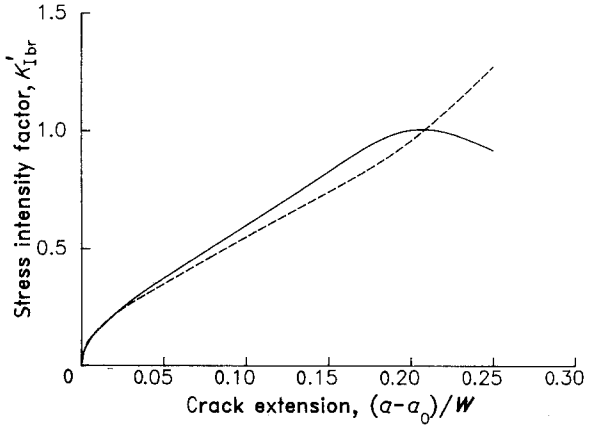

Figure 7 Bridging stress intensity factor as a function of crack extension: (——) constant-load test, (– – –) test with constant $K'_{I\,tip}$.

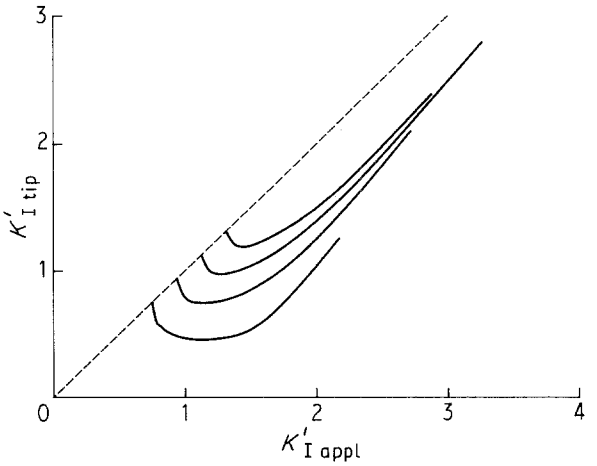

Figure 8 Development of the crack-tip stress intensity factor $K'_{I\,tip}$ in constant-load tests.

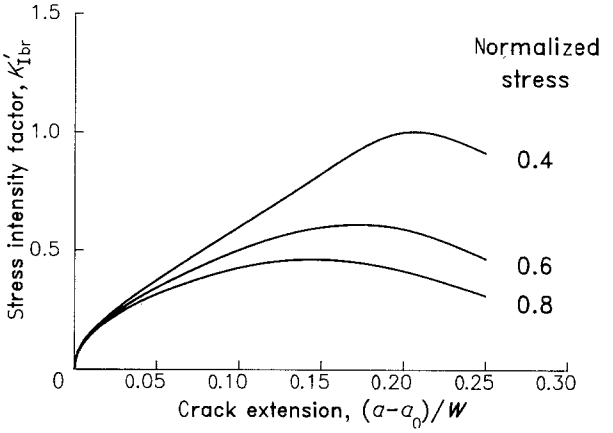

Figure 9 Development of the R-curve stress intensity factor $K'_{I\,br}$ in constant load tests (normalized stress = σ/σ_0).

The bridging stress intensity factor $K_{I\,br}$ is plotted in Fig. 11 against $\Delta a/W$. In this representation the dependency on $K_{I\,tip}$ becomes more obvious. It can be seen from Figs 6, 7, 9, 10 and 11 that the bridging stress intensity factor $K_{I\,br}$ shows a square-root shaped increase for small crack extensions. This can easily be understood. If the crack extension is small compared with the initial notch depth $\Delta a = a - a_0 \ll a_0$, the displacements δ_{total}, δ_{appl} and δ_{br} are also small within the whole range $a_0 \leq x \leq a$. In this case $\delta \ll \delta_{00}$ and consequently $\sigma_{br} \simeq \sigma_0$.

In this special case the application of the weight function yields the bridging stress intensity factor

$$K_{I\,br} = \left(\frac{8a}{\pi}\right)^{1/2} \sigma_0 \left[\left(1 - \frac{a_0}{a}\right)^{1/2} + \sum A_{\mu\nu} \frac{1}{2\nu + 3} \times \frac{(a/W)^{\mu}}{[1-(a/W)]^{3/2}} \left(1 - \frac{a_0}{a}\right)^{\nu+(3/2)}\right] \quad (15)$$

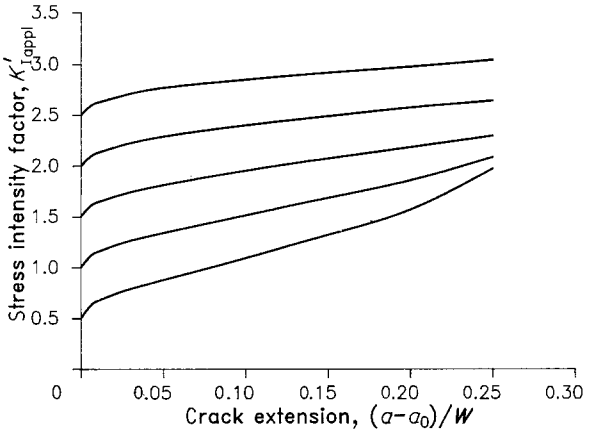

Figure 10 R-curves for crack extension with constant crack-tip stress intensity factors $K_{I\,tip}$.

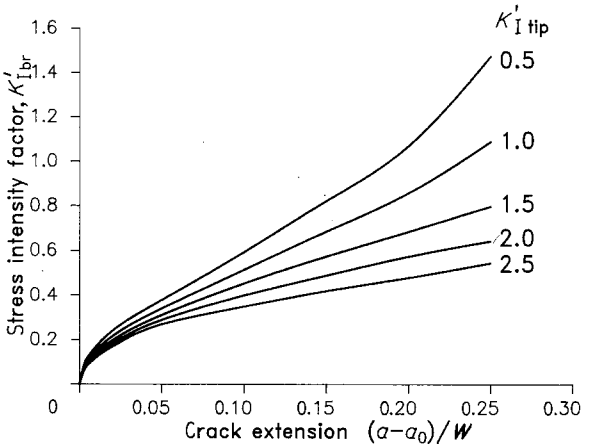

Figure 11 Development of the bridging stress intensity factor $K_{I\,br}$ for crack extension tests with constant crack-tip stress intensity factor $K_{I\,tip}$.

Since for $\Delta a \rightarrow 0$ in Equation 15 only the first term in brackets contributes to the bridging stress intensity factor, we have

$$K_{I\,br} = \sigma_0 \left(\frac{8\Delta a}{\pi}\right)^{1/2} \tag{16}$$

and the square-root shaped increase in the bridging stress intensity factor with crack extension becomes obvious.

5. Determination of bridging stress parameters from literature results

In this section, the weight-function based procedure described above is applied to determine the parameters (σ_0, δ_{00}) of the bridging stress law from experimental data available in the literature. For the evaluation Equation 5.2 is assumed to be valid.

5.1. Stable crack propagation

First stable crack propagation under increasing load is considered. Fig. 12 shows a set of R-curves for 99.8% Al_2O_3 with a mean grain size of $\simeq 16\,\mu m$ [4]. The original data expressed by energy release rates

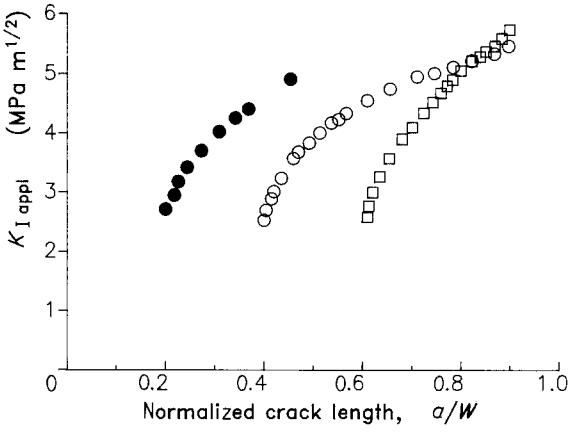

Figure 12 R-curves for coarse-grained Al_2O_3 based on measurements of Steinbrech and Schmenkel [4]. Different symbols denote different specimens.

were converted by

$$K_{I\,appl} = \left(\frac{GE}{1-\nu^2}\right)^{1/2} \tag{17}$$

($E = 360$ GPa, $\nu = 0.22$) into applied stress intensity factors $K_{I\,appl}$. The crack-tip stress intensity factor $K_{I\,tip}$ in the stable crack growth test is given by the initial value of $K_{I\,appl}$ at $\Delta a = 0$. Due to the approximately square-root-shaped R-curves for $\Delta a \rightarrow 0$, this value can hardly be measured in a stable crack growth test. Therefore, the value of K_{I0} has also to be considered to be an unknown parameter.

In order to determine the unknown parameters σ_0, δ_{00}, K_{I0}, a least-squares procedure was applied for the R-curve with $a_0/W = 0.4$:

(i) The procedure starts with an arbitrarily chosen set of the parameters σ_0, δ_{00}, K_{I0}. For the given value K_{I0} the corresponding applied stress σ_{appl} is given by

$$K_{I0} = \int_0^{a_0} h\left(\frac{x}{a}, \frac{a}{W}\right) \sigma_{appl}\, dx \tag{18}$$

In the case of a bending bar the applied stress becomes

$$\sigma_{appl} = \hat{\sigma}_{appl}\left(1 - 2\frac{x}{W}\right) \tag{19}$$

where $\hat{\sigma}_{appl}$ is the outer fibre bending stress.

(ii) Solution of the set of Equations 10, 7.1, 7.2 and 1 provides the stress intensity factors $K_{I\,appl}$, $K_{I\,br}$ and $K_{I\,tip}$. In this way, one obtains the calculated R-curve

$$K_{I\,appl,\,calc} = f(a/W, \sigma_0, \delta_{00})$$

for the actual parameter set.

(iii) The least-squares routine compares the calculated R-curve with the experimental R-curve and determines the sum of squares according to

$$S^2 = \sum (K_{I\,appl,\,calc} - K_{I\,appl,\,exp})^2 \tag{20}$$

The routine changes the parameter set $(\sigma_0, \delta_{00}, K_{I0})$ until a minimum of S^2 is reached. So the best parameter set in least-squares terms is determined. For practical use the authors applied the Harwell routine VA02A.

As a result of this procedure it was found for $m = 1$

$\delta'_{00} = 0.5 \quad K'_{\mathrm{Itip}} = 0.69 \quad K_{\mathrm{I0}} = 2.4\ \mathrm{MPa\,m^{1/2}}$

and with $W = 7$ mm

$$\sigma_0 = 42\ \mathrm{MPa} \qquad \delta_{00} = 0.41\ \mu\mathrm{m}$$

The fitting curve corresponding to these parameters is plotted in Fig. 13 as a solid line. Using this parameter set the R-curves for $a_0/W = 0.2$ and 0.6 were also calculated. The results are plotted in Fig. 13 as dashed lines. The agreement is excellent for $a_0 = 0.6$, and also for $a_0/W = 0.2$ the experimental results can be well described, but for large crack extension deviations are evident.

Since the bridging stress parameters are known, the crack surface profile results from Equation 10. Fig. 14 shows the crack profile for the crack with $a_0/W = 0.4$ after a crack propagation of $\Delta a/W = 0, 0.1, 0.2$ and 0.3. The crack surface profiles exhibit square-root-shaped near-tip displacements which are directly proportional to the crack-tip stress intensity factor K_{Itip}. The corresponding distribution of the bridging stresses $\sigma_{\mathrm{br}}(x)$ is shown in Fig. 15.

It should be mentioned in this context that the procedure presented, based on the fracture-mechanical weight function, does not require any additional assumption to be made on a special crack opening

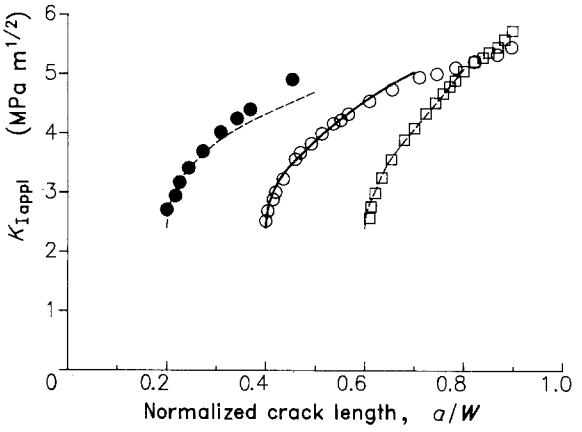

Figure 13 R-curves of Fig. 12 compared with curves calculated with the parameters from the least-squares procedure: (——) fitted R-curve, (– – –) predicted R-curves. Different symbols denote different specimens.

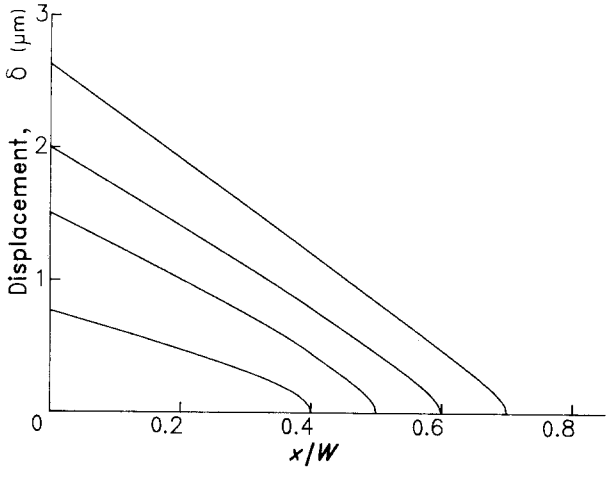

Figure 14 Crack surface profiles according to Fig. 13; $a_0/W = 0.4$.

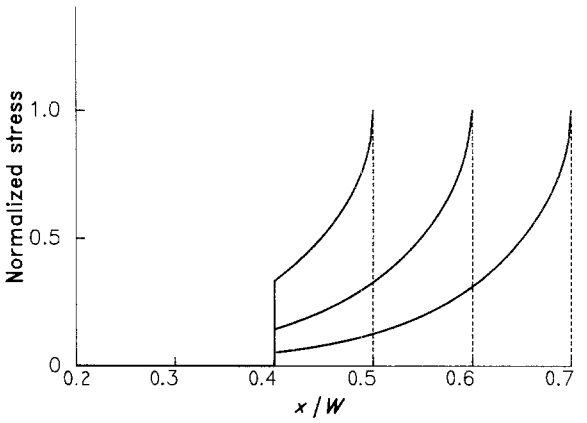

Figure 15 Bridging stresses for cracks with different crack extensions (lines as in Fig. 14; $a_0/W = 0.4$).

profile, as for example applied in the J-integral evaluation performed by Steinbrech *et al.* [22].

5.2. Subcritical crack extension

A second possibility of determining the parameters of Equation 5.2 is the evaluation of subcritical crack growth measurements. Results of crack growth measurements for alumina from specimens with macrocracks are reported in [9]. Two commercially available materials were investigated:

(i) Material I: 99.6% Al_2O_3, $K_{\mathrm{Ic}} = 3.3\ \mathrm{MPa\,m^{1/2}}$, average grain size 20 μm.

(ii) Material II: 99.6% Al_2O_3 (HIPped), $K_{\mathrm{Ic}} = 4\ \mathrm{MPa\,m^{1/2}}$; this material shows an inhomogeneous grain size distribution with a mean grain size of 3.2 μm and maximum grains of $\simeq 25$ μm size.

The results reported [9] were obtained with single-edge notched specimens, 3.5 mm × 4.5 mm × 50 mm in size, loaded in three-point bending with a constant load. The notch in the centre of the specimen was prepared with a diamond saw. The notch depth was 2.245 ± 0.01 mm, the notch width 50 μm.

In Figs 16 and 17 $\mathrm{d}a/\mathrm{d}t$–K_{Iappl} curves are plotted for different stresses applied. Two types of $\mathrm{d}a/\mathrm{d}t$–K_{I}-curves can be seen. First, a decrease of the crack growth rate with increasing crack length and therefore increasing K_{Iappl} is obvious. The crack growth rate drops by several orders of magnitude within a small amount of crack extension. After a large range with a nearly constant crack growth rate the crack growth rate increases until final fracture. For the lowest K_{Ii} for both materials crack arrest was observed.

Whilst in the case of stable crack extension the value K_{Itip} is known, the crack-tip stress intensity factor changes during crack propagation in constant-load tests. In order to determine the parameters σ_0, δ_{00} from such tests, a least-squares procedure is again applied. The treatment is outlined for the special case where the subcritical crack growth is described by a power-law relation

$$v = \frac{\mathrm{d}a}{\mathrm{d}t} = AK_{\mathrm{I}}^n = A^*(K_{\mathrm{I}}/K_{\mathrm{Ic}})^n \qquad (21)$$

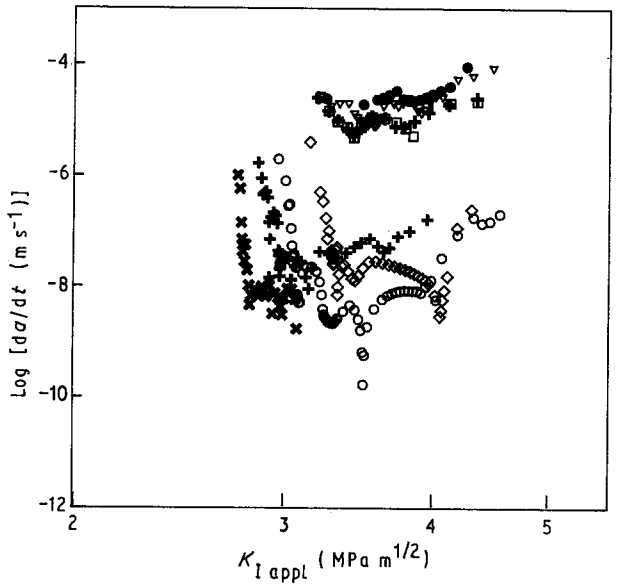

Figure 16 v–K_I curves for specimens with macrocracks from static bending tests (material I) [9]; K_{Ii} = 2.72/2.96/3.06/2.82/3.20/3.21/3.25 MPa $m^{1/2}$.

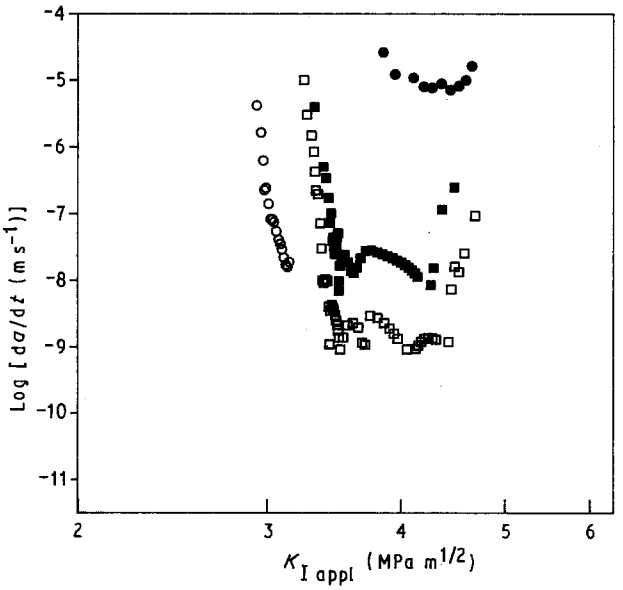

Figure 17 v–K_I curves for specimens with macrocracks from static bending tests (material II) [9]; K_{Ii} = 2.93/3.25/3.32/3.85 MPa $m^{1/2}$.

(i) The procedure starts with an estimated initial combination of parameters (σ_0, δ_{00}, A^*, n). For any data point ($K_{I\text{appl}}$, a/W) the crack tip stress intensity factor $K_{I\text{tip}}$ is calculated, and using Equation 21 the subcritical crack growth rate v_{calc} is calculated.

(ii) The calculated and the measured crack growth rates v_{meas} are compared and the sum of squares is determined by

$$S^2 = \sum (\log v_{\text{calc}} - \log v_{\text{meas}})^2 \qquad (22)$$

(iii) Further treatment by the least-squares procedure is similar to that for stable crack propagation apart from the fact that now a set of four parameters are determined.

The result of calculation is

Material I: σ_0 = 46.4 MPa, δ_{00} = 0.95 μm,

$\log A^*$ = − 2.97, n = 25

Material II: σ_0 = 88.8 MPa, δ_{00} = 0.224 μm,

$\log A^*$ = − 0.7, n = 25

In earlier investigations the subcritical crack growth behaviour of natural cracks was determined for material I [23] and material II [24] by application of a modified lifetime method [25] ignoring possible R-curve effects. The result was n = 38 for material I and n = 20 for material II. The discrepancies in the n values for the macro-cracks may be caused either by fundamental differences in the subcritical crack growth behaviour of natural, small cracks compared with artifical macro-cracks and/or by intolerable influences of the R-curve on the evaluation procedure for the natural cracks.

To check the accuracy of the parameters determined (σ_0, δ_{00}, A^*, n), the least-squares sums S^2 – normalized to the minimum value $S^2_{\min}$ – are plotted in Fig. 18 for a number of power-law exponents n. The dashed line represents δ'_{00} and the dash-dotted curve shows σ_0.

In Fig. 19 the v–$K_{I\text{appl}}$ curves – calculated with the bridging parameters of material II – are plotted for

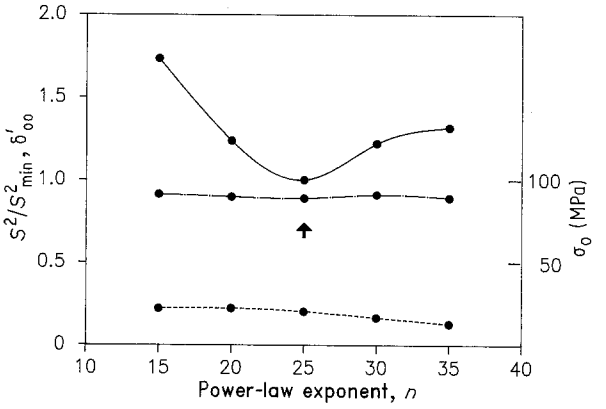

Figure 18 Least-squares results for fixed exponents n: (——) $S^2/S^2_{\min}$ (left-hand scale), (– – –) δ'_{00} (left-hand scale), (— · —) σ_0 (right-hand scale); material II.

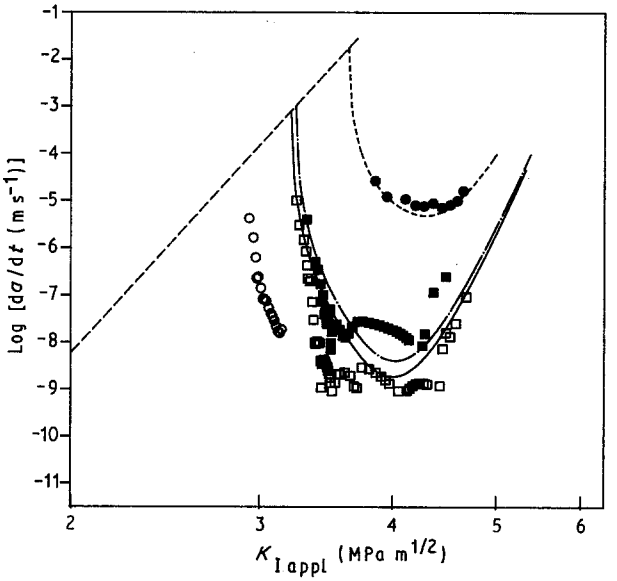

Figure 19 v–$K_{I\text{appl}}$ curves for material II calculated with the fitted parameter set (dashed straight line: $v = f(K_{I\text{tip}})$).

several initial stress intensity factors K_{Ii}. The dashed straight line describes the power-law relation $v = AK_{Itip}^{n}$. Finally, Fig. 20 shows the R-curve calculated with the fitted material data. A comparison of the σ–δ relations obtained for the three materials is given in Fig. 21.

6. R-curve for natural cracks

In this section it is assumed that the bridging stresses determined with macro-cracks can be applied also to natural cracks. It is of special interest how the bridging stresses affect the strength and the lifetimes of specimens with a natural flaw population. The natural cracks are modelled by semicircular surface cracks ignoring special surface influences, i.e. by a half of an embedded circular crack. As illustrated in Fig. 22, the initial crack size is a_0 and the actual crack size is a. The displacements due to the radial stress distribution $\sigma(r)$ are described by [26]

$$\delta(r) = \frac{4(1-\nu^2)}{\pi E} a \int_{\rho}^{1} \frac{1}{(x^2-\rho^2)^{1/2}} \times \left[\int_{0}^{x} \frac{\rho\sigma d\rho}{(x^2-\rho^2)^{1/2}} \right] dx \quad \rho = r/a \qquad (23)$$

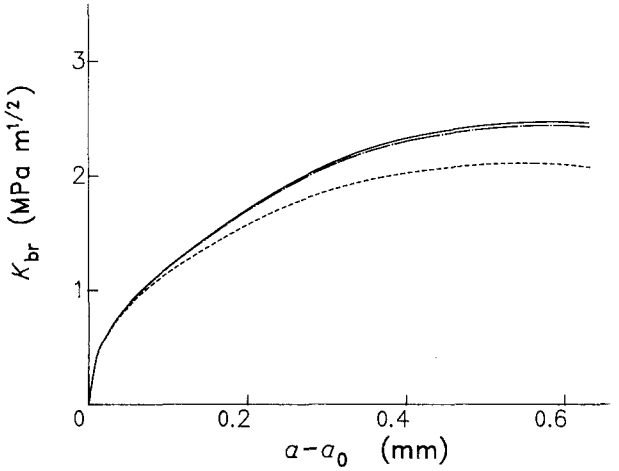

Figure 20 R-curves for material II calculated with the fitted parameter set and $K_{Ii} = 4$ MPa m$^{1/2}$. Lines as in Fig. 19; K_{Ii} (MPa m$^{1/2}$) = (——) 3.25, (— · —) 3.32, (– – –) 3.85.

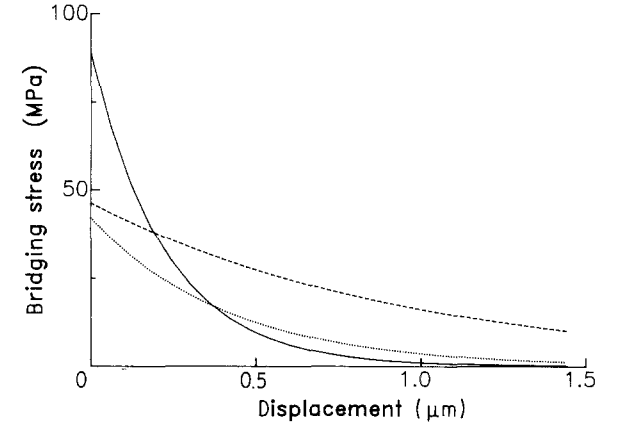

Figure 21 Bridging stress relations for the three materials investigated: (– – –) material I, (——) material II, (· · ·) Al_2O_3 (from [4]).

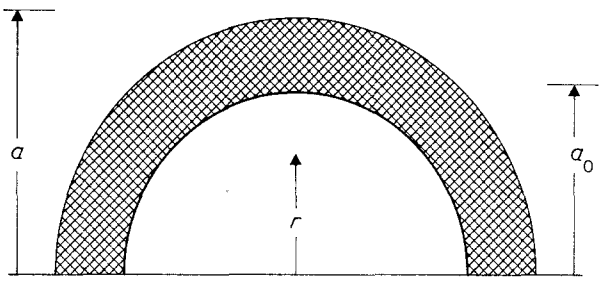

Figure 22 Semicircular crack.

where x is a dimensionless integration variable. The related stress intensity factor is given by

$$K_I = \frac{2}{(\pi a)^{1/2}} \int_0^a \frac{r\sigma(r)\,dr}{(a^2-r^2)^{1/2}} \qquad (24)$$

6.1. Analytical solutions for special cases

The crack surface displacement under homogeneously distributed stress $\sigma = \sigma_{appl} = \text{const.}$ is

$$\delta_{appl} = \frac{4(1-\nu^2)}{\pi E} \sigma_{appl}(a^2-r^2)^{1/2} \qquad (25)$$

and the stress intensity factor

$$K_{Iappl} = \frac{2}{\pi^{1/2}} \sigma_{appl} a^{1/2} \qquad (26)$$

The maximum displacement (occurring at $r = 0$) is

$$\delta_{appl,r=0} = \frac{4(1-\nu^2)}{\pi E} \sigma_{appl} a = \frac{2(1-\nu^2)}{\pi E} K_{Iappl} a^{1/2} \qquad (27)$$

For a crack with $a = 100$ μm and $E = 360$ GPa we obtain a maximum displacement when K_{Iappl} reaches K_{I0}. With a value of $K_{I0} = 3$ MPa m$^{1/2}$ – typical of coarse-grained Al_2O_3 – one obtains

$$\delta_{appl,max} = 0.09\ \mu\text{m}$$

If we compare this limit value with the characteristic displacements δ_{00} and if we keep in mind that

(i) the displacements decrease from the crack origin to the crack-tip, and

(ii) the bridging stresses will reduce the crack opening,

we can realize that the relevant crack surface displacements are small compared with the values of δ_{00}. This will at least hold for material I. Consequently, one can approximate

$$\sigma_{br} \simeq \sigma_0$$

For material II, where δ_{00} is of the same order of magnitude as the displacements in the bridging zone, this approximation will lead to an upper-limit case for the R-curve of the natural cracks. With this simplification made, the bridging stress intensity factor obtained from Equation 24 is

$$K_{Ibr} = \frac{2}{(\pi a)^{1/2}} \sigma_0 (a^2 - a_0^2)^{1/2} \qquad (28)$$

The crack surface displacement due to the bridging

stresses is given by [27]

$$\delta_{appl} = \delta^* \frac{4(1-\nu^2)a\sigma_0}{\pi E} \tag{29}$$

with

$$\delta^* = \int_{r/a}^{a_0/a} \frac{x\,dx}{[x^2-(r/a)^2]^{1/2}} + \int_{a_0/a}^{1} \times \frac{x-[x^2-(a_0/a)^2]^{1/2}}{[x^2-(r/a)^2]^{1/2}}\,dx \quad \text{for } r < a_0 \tag{30a}$$

$$\delta^* = \int_{a/r}^{1} \frac{x-[x^2-(a_0/a)^2]^{1/2}}{[x^2-(r/a)^2]^{1/2}}\,dx \quad \text{for } r > a_0 \tag{30b}$$

or in an analytically integrated form

$$\delta^* = \left[1-\left(\frac{r}{a}\right)^2\right]^{1/2}\left[1-\left(\frac{a_0}{a}\right)^2\right]^{1/2} - \frac{a_0}{a}\left\{\boldsymbol{E}(r/a_0) - E[\sin^{-1}(a_0/a),(r/a_0)]\right\} \quad \text{for } r < a_0 \tag{30c}$$

and

$$\delta^* = \left[1-\left(\frac{r}{a}\right)^2\right]^{1/2}\left[1-\left(\frac{a_0}{a}\right)^2\right]^{1/2} - \frac{r}{a}\left(\boldsymbol{E}(a_0/r) - E[\sin^{-1}(r/a, a_0/r)] - \left[1-\frac{a_0^2}{r^2}\right]\{\boldsymbol{K}(a_0/r) - F[\sin^{-1}(r/a),(a_0/r)]\}\right) \quad \text{for } r > a_0 \tag{30d}$$

where F and E are the first and second elliptical integrals and $\boldsymbol{K}$ and $\boldsymbol{E}$ are the corresponding complete elliptical integrals. In this context, it should be mentioned that the solution given by Sneddon [26], namely

$$\delta^* = [1-(r/a)^2]^{1/2}[1-(a_0/a)^2]^{1/2} \tag{31}$$

is wrong [27].

Fig. 23 shows the displacements caused by the bridging stresses in a normalized representation. In Fig. 24 the R-curve according to Equation 28 is plotted for the natural cracks. In a strength test only a small part of this curve will be covered. The points of instability where the strength is reached (material I: 220 MPa, material II: 370 MPa) are marked by solid circles.

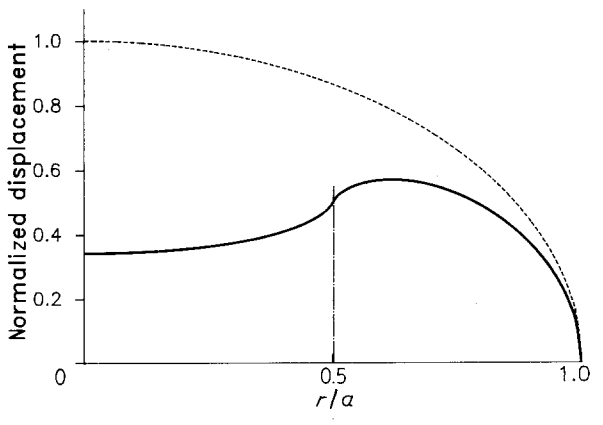

Figure 23 Displacements due to bridging stresses (normalized displacement = $-\delta^*$) for (——) $a_0/a = 0.5$ and (– – –) $a_0/a = 0$.

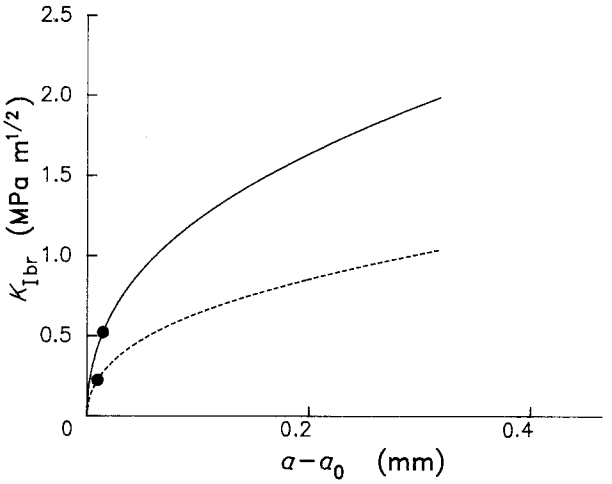

Figure 24 R-curves for the natural cracks: (– – –) material I, (——) material II, (●) locations of failure; $a_0 = 0.1$ mm.

6.2. Influence of bridging stresses on strength

The critical stress σ_c (the strength) results from the two conditions

$$K_{I0} = K_{Iappl} - K_{Ibr}(\Delta a) \qquad \left(\frac{\partial K_{Iappl}}{\partial a}\right)_{\sigma=\text{const}=\sigma_c} = \frac{dK_{Ibr}}{d(\Delta a)} \tag{32}$$

Fig. 25 represents the strength influenced by the bridging stresses as a function of the strength when no bridging effect occurs. The range of experimentally determined strength data according to Figs 26 and 27 is introduced in Fig. 25. The influence of the R-curve on the strength of specimens with natural flaw population is small, which can be concluded from Fig. 25.

6.3. Influence of bridging stresses on lifetimes

The lifetime t_f in a static test performed with the stress σ results in

$$t_f = \int_{a_0}^{a_c} \frac{da}{v} = \frac{1}{A}\int_{a_0}^{a_c} \frac{da}{(\sigma Y a^{1/2} - K_{Ibr})^n} \tag{33}$$

where a_0 is the initial value of the crack length a and a_c is the crack length at failure. Under subcritical crack growth conditions the crack size at failure a_c can be derived from a failure condition analogous to Equation 32 for the applied stress σ.

In Fig. 28 the influence of the bridging stresses on the lifetimes is illustrated. The comparison between the lifetimes in the presence of bridging stresses and lifetimes in the absence of bridging stresses shows longer lifetimes as a consequence of the bridging stresses. Also a lower slope of the curve with bridging

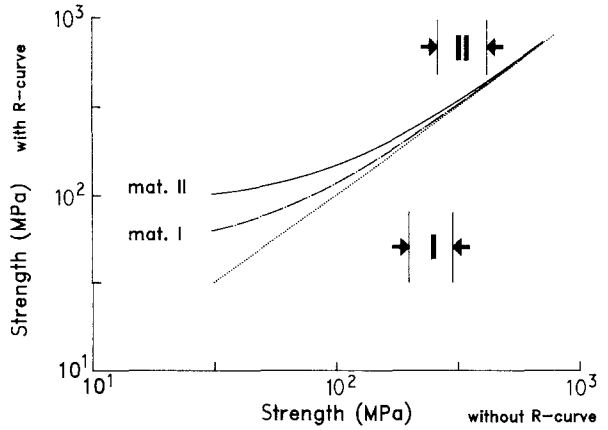

Figure 25 Influence of bridging stresses on the inert strength.

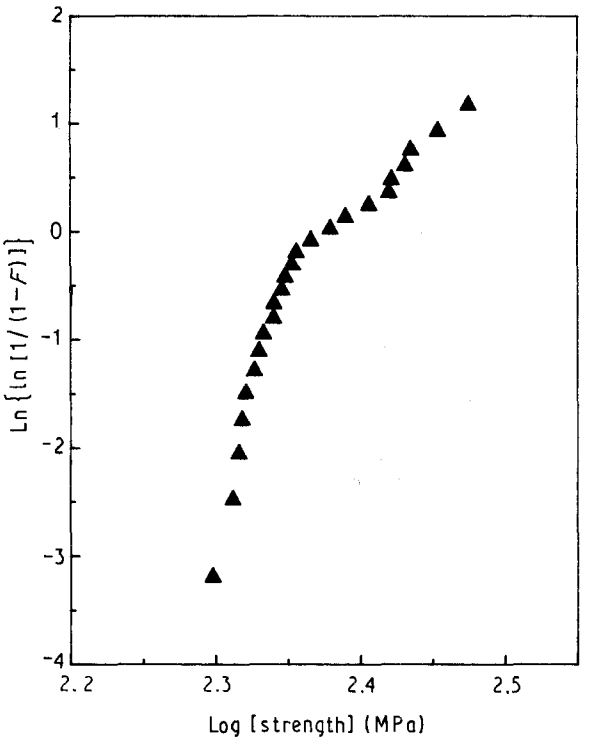

Figure 26 Four-point bending strength of material I. [23].

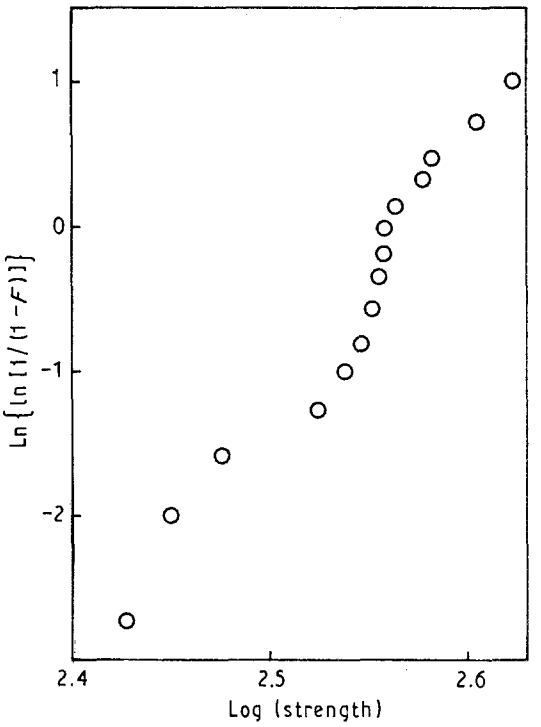

Figure 27 Four-point bending strength of material II. [28].

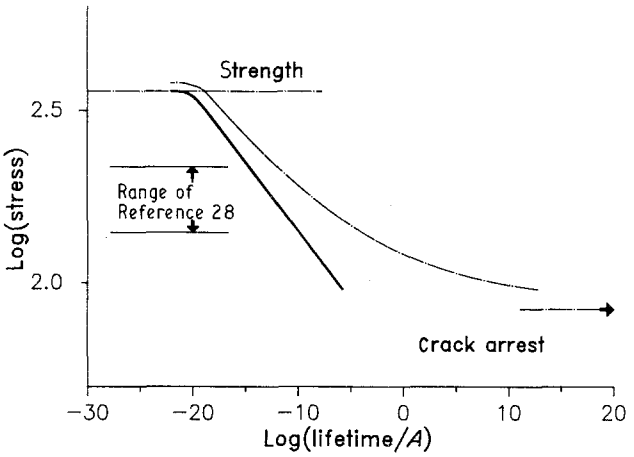

Figure 28 Influence of bridging stresses on the lifetime in static tests (material II): (——) without and (—·—) with bridging stresses.

stresses is evident [28]. This will lead to an increased exponent of the power law $t_f \propto \sigma^{-n}$. The slightly different strength values can also be seen in Fig. 28.

6.4. A procedure to determine bridging stresses for natural cracks

It cannot be excluded that bridging behaviour of natural cracks may deviate from the behaviour of macrocracks. Therefore, it is desirable to determine the bridging stress relation for natural cracks. In the case where the lifetimes are affected by the bridging stresses, it should – in principle – be possible to determine these stresses from lifetime measurements. A possible procedure – based on strength and lifetime measurements in static tests – is described below:

1. At the beginning of the procedure a least-squares routine provides an arbitrary set of parameters A, n for a power-law description of subcritical crack growth and σ_0, δ_{00}, m for a three-parametric bridging relation (e.g. Equations 5.1–5.3).

2. For each measured strength value σ_{cv} the related initial crack size a_{0v} is determined from the failure conditions in strength tests

$$K_{I\text{appl}} = \sigma_{cv} Y a_{cv}^{1/2} = K_{I0} + K_{I\text{br}}|_{a_{cv}-a_{0v}} \quad Y \simeq 2/\pi^{1/2} \times \left(\frac{\partial K_{I\text{appl}}}{\partial a_{cv}}\right)_{\sigma=\text{const}} = \frac{\mathrm{d}K_{I\text{br}}}{\mathrm{d}a_{cv}} \tag{34}$$

3. Lifetime computations:

(a) Calculation of the final crack length a_c in a constant load test using Equation 32 for the stress occurring in the tests.

(b) In the next step the integral equation (resulting from combination of Equations 5 and 23) has to be

solved. Especially for the case $m = 1$ it yields

$$\log \frac{\sigma_{br}}{\sigma_0} + \frac{4(1-\nu^2)}{\pi E \delta_{00}} a \int_\rho^1 \frac{1}{(x^2-\rho^2)^{1/2}} \times \left[\int_0^x \frac{\rho \sigma \, d\rho}{(x^2-\rho^2)^{1/2}} \right] dx = 0 \quad (35)$$

The solution of this integral equation can be determined by successive approximation. The result is the radial distribution of the bridging stresses over the crack.

(c) Equation 24 then provides the bridging stress intensity factor K_{Ibr}.

(d) Now, all information is available to evaluate the lifetime relation

$$t_{f\,calculated} = \frac{1}{A} \int_{a_0}^{a_c} \frac{da}{(\sigma Y a^{1/2} - K_{Ibr})^n} \quad (36)$$

4. The calculated lifetimes are then compared with the measured ones corresponding to the same failure probability and the sum of squares is determined as

$$S^2 = \sum (\log t_{f\,calculated} - \log t_{f\,measured})^2 \quad (37)$$

5. In the next step the parameter set is changed systematically and the procedure starts again from point 1 with these new parameters.

6. The procedure is repeated until the squares S^2 reach a minimum.

The result is the best parameter set for description of the v–K_I curve and bridging relation.

Lifetime calculations according to the procedure proposed above require the solution of Equation 35 for any crack growth increment da during evaluation of Equation 36. In order to reduce the effort in determination of the bridging stress intensity factors, Equation 35 has been solved numerically [14] for several values of the parameters δ_{00}, a_0/a, K_{Itip}.

7. Conclusions

The R-curve effect caused by bridging stresses between the crack surfaces has been analysed by application of the fracture-mechanical weight function. Exponential relations describing the macroscopically averaged bridging stresses have been derived, and the related R-curves have been calculated for conditions of subcritical and stable crack propagations. Crack growth data from the literature were used to determine the parameters of the bridging relation by a least-squares procedure.

By use of the bridging stresses obtained in macrocrack tests the influence on strength and lifetime could also be studied for small natural cracks. Finally, a procedure is proposed to determine the parameters of the bridging stress relation from strength data and lifetimes in static tests.

References

1. H. HÜBNER and W. JILLEK, *J. Mater. Sci.* **12** (1977) 117.
2. R. KNEHANS and R. W. STEINBRECH, *J. Mater. Sci. Lett.* **1** (1982) 327.
3. R. W. STEINBRECH, R. KNEHANS and W. SCHAARWÄCHTER, *J. Mater. Sci.* **18** (1983) 265.
4. R. STEINBRECH and O. SCHMENKEL, *Commun. J. Amer. Ceram. Soc.* **71** (1988) C271.
5. E. K. BEAUCHAMP and S. L. MONROE, *J. Amer. Ceram. Soc.* **72** (1989) 1179.
6. D. G. JENSEN, V. ZELIZKO and M. V. SWAIN, *J. Mater. Sci. Lett.* **8** (1989) 1154.
7. A. OKADA, N. HIROSAKI and M. YOSHIMURA, *J. Amer. Ceram. Soc.* **73** (1990) 2095.
8. P. L. SWANSON, C. J. FAIRBANKS, B. R. LAWN, Y. MAI and B. J. HOCKEY, *ibid.* **70** (1987) 279.
9. T. FETT and D. MUNZ, *ibid.* **75** (1992) 958.
10. G. VEKINIS, M. F. ASHBY and P. W. R. BEAUMONT, *Acta Metall. Mater.* **38** (1990) 1151.
11. H. FREI and G. GRATHWOHL, *Ceram. Forum Internat.* **67** (1991) 27.
12. J. RÖDEL, J. F. KELLY and B. R. LAWN, *J. Amer. Ceram. Soc.* **73** (1990) 3313.
13. Y. MAI and B. R. LAWN, *ibid.* **70** (1987) 289.
14. T. FETT and D. MUNZ, "Evaluation of R-curve effects in ceramics caused by bridging interactions", KfK Report 4940 (Kernforschungszentrum Karlsruhe, 1991).
15. H. BÜCKNER, *ZAMM* **50** (1970) 751.
16. J. R. RICE, *Int. J. Solids Struct.* **8** (1972) 751.
17. T. FETT and D. MUNZ, *J. Mater. Sci. Lett.* **9** (1990) 1403.
18. P. C. PARIS, Document D2-2195 (Boeing Co., 1957).
19. H. TADA, "The Stress Analysis of Cracks Handbook" (Del Research Corp., 1986).
20. T. FETT, "Stress intensity factors and weight functions for the edge cracked plate calculated by the Boundary Collocation Method", KfK-Report 4791 (Kernforschungszentrum Karlsruhe, 1990).
21. M. SAKAI, J. YOSHIMURA, Y. GOTO and M. INAGAKI, *J. Amer. Ceram. Soc.* **71** (1988) 609.
22. R. STEINBRECH, A. REICHL and W. SCHAARWÄCHTER, *ibid.* **73** (1990) 2009.
23. T. FETT and MUNZ, in Proceedings of 7th CIMTEC, June 1990, editor P. Vincencini (Elsevier Science, 1991) pp. 1827–1835.
24. T. FETT, K. KELLER and D. MUNZ, NAGRA Technical Report 85-51 (Baden, Switzerland, 1985).
25. T. FETT and D. MUNZ, *Commun. Amer. Ceram. Soc.* **68** (1985) C213.
26. I. N. SNEDDON, *Proc. R. Soc. London* **A** 187 (1946) 229.
27. T. FETT, *Int. J. Fract.* **20** (1982) R135.
28. T. FETT and D. MUNZ, in Proceedings, "Fracture Mechanics of Ceramics", Nagoya, 1991, Vol. 9, 1992, p. 219.

Received 16 September 1991
and accepted 2 June 1992